

Velde: constructing cell potential landscapes by RNA velocity vector field decomposition

Junbo Jia¹ , Luonan Chen^{1,2*}

¹Key Laboratory of Systems Health Science of Zhejiang Province, School of Life Science, Hangzhou Institute for Advanced Study, University of Chinese Academy of Sciences, Hangzhou 310024, China

²Center for Excellence in Molecular Cell Science, Shanghai Institute of Biochemistry and Cell Biology, Chinese Academy of Sciences, Shanghai 200031, China

(November 20, 2023)

Abstract

The Waddington landscape serves as a metaphor illustrating the developmental process of cells, likening it to a small ball rolling down various trajectories into valleys. Constructing an epigenetic landscape of this nature aids in visualizing and gaining insights into cell differentiation. Development encompasses intricate processes involving both cell differentiation and cell cycles. However, current landscape methods solely focus on constructing a potential landscape for cell differentiation, neglecting the accompanying cell cycle. This paper introduces a novel method that simultaneously constructs two types of potential landscapes using single-cell RNA sequencing data. Specifically, it presents the natural Helmholtz-Hodge decomposition (nHHD) of a continuous vector field within a bounded domain in n -dimensional Euclidean space. This decomposition uniquely breaks down the vector field into a gradient field, a rotation field, and a harmonic field. Utilizing this approach, the RNA velocity vector field is separated into a curl-free component representing cell differentiation and a curl component representing the cell cycle. By calculating the corresponding potential functions, potential landscapes for both cell differentiation and the cell cycle are obtained. Finally, the efficacy of this method is demonstrated through its application to synthetic and real datasets.

Key words: scRNA-seq; RNA velocity; Potential landscape; Helmholtz decomposition

1 Introduction

The invention of single-cell RNA sequencing (scRNA-seq) has enabled the study of cell heterogeneity in tissues and the development of cells at the resolution of individual cells [Tang et al., 2009, Eberwine et al., 2014]. Particularly in medical research, scRNA-seq allows for more precise targeting of immunotherapy or targeted therapy towards specific cells or cell subpopulations [Rood et al., 2022, H. et al., 2020, Lim et al., 2023]. Consequently, scRNA-seq holds significant potential for broader application in analyzing biological functional mechanisms and discovering more effective methods for disease treatment.

scRNA-seq captures a snapshot of cell development, enabling the inference of developmental trajectories as one of the primary downstream analysis tasks (the other being cell subpopulation identification through clustering) [Luecken and Theis, 2019]. By utilizing first principles, dynamic modeling of mRNA splicing during gene expression can yield RNA velocity, allowing for the determination of each cell's developmental direction in the near future [La Manno et al., 2018], as

*Corresponding author. Email address: lnchen@sibcb.ac.cn

depicted in Figure 1ABC. Furthermore, leveraging reconstruction methods for continuous vector fields, such as sparse vector field consensus (sparse VFC) [Ma et al., 2013], enables the construction of a comprehensive RNA velocity vector field, as illustrated in Figure 1D, offering an analytical approach to studying cell state transitions [Qiu et al., 2022].

The Waddington landscape, proposed in 1957, offers an elementary and intuitive description of cell development [Waddington, 1957]. It draws an analogy between the development of cells and a small ball rolling along various tracks from a mountain slope to a valley. This analogy vividly portrays cell differentiation as the process of small balls selecting different tracks. In fact, this landscape assigns each cell a differentiation potential energy, where cells at higher elevations possess greater differentiation potential energy compared to cells at lower altitudes. This suggests that cells with higher potential have the ability to differentiate into cells with lower potential energy [Teschendorff and Feinberg, 2021]. Currently, there exist several methods for quantifying cell potency and inferring the differentiation trajectory of cells from scRNA-seq data. Some graph-based methods include Wishbone [Setty et al., 2016], Diffusion pseudotime [Haghverdi et al., 2016], Monocle/Monocle2 [Trapnell et al., 2014, Qiu et al., 2017] scEpath [Jin et al., 2018], and other. Additionally, there are entropy-based methods such as StemID [Grün et al., 2016], SLICE [Guo et al., 2017b], SCENT [Teschendorff and Enver, 2017], and Markov chain entropy [Shi et al., 2020]. Moreover, dynamic modeling-based methods like PBA [Tusi et al., 2018] and LDD [Shi et al., 2019] are also available.

Although numerous methods exist for quantifying cell potency, constructing a Waddington-like landscape to illustrate cell development still poses a challenge. Some approaches aim to build such landscapes based on gene regulatory networks (GRNs) [Wang et al., 2010, Guo et al., 2017a], but they are constrained by the availability of prior information on gene regulation and the limited number of genes considered. Moreover, these methods are not applicable to real scRNA-seq data. In this article, we present a novel method that addresses these limitations by simultaneously constructing two landscapes: the cell differentiation landscape and the cell cycle landscape, using scRNA-seq data. We posit that the heterogeneity of cells primarily arises from two concurrent processes: transition and cycle, as illustrated in Figure 1E. Transition can be described as a cell changing from one state to another, such as during differentiation and dedifferentiation. Meanwhile, cycle is described as the cell rotating around its state. Building on this assumption, we extend the natural Helmholtz-Hodge decomposition method in 2- and 3-dimensional space [Bhatia et al., 2014] to n -dimensional space, and employ this method to decompose the RNA velocity vector field into the sum of a gradient vector field and a rotating vector field, which describe cell transition and cycle, respectively, in order to derive their differentiation potential landscape and cell cycle potential landscape, as depicted in Figure 1F. This method is termed *Velde*, signifying its principle is to construct distinct potential landscapes through RNA Velocity vector field decomposition. Finally, we validate the effectiveness of this method using both synthetic and real datasets.

The rest of the paper is organized as follows. In section 2, the underlying theory and constructing process of landscapes was provided. In section 3, the effectiveness of our method was verified using different datasets. Finally, conclusions and discussions was given in section 4.

2 Methods

Before delving into the specific process of *Velde*, let us first introduce the underlying theory.

2.1 The natural Helmholtz-Hodge decomposition of n -dimensional vector field

Here we first propose the natural Helmholtz-Hodge decomposition (nHHD) of vector fields in an n -dimensional bounded domain, which is the cornerstone of our method *Velde*. The nHHD is based on two works. First, Glötzl Erhard and Richters Oliver considered the rotation as a superposition of $\binom{n}{2}$ rotations within the coordinate planes and extend the Helmholtz-Hodge decomposition to vector fields in n -dimensional Euclidean space [Glötzl and Richters, 2020]. Second, Bhatia Harsh

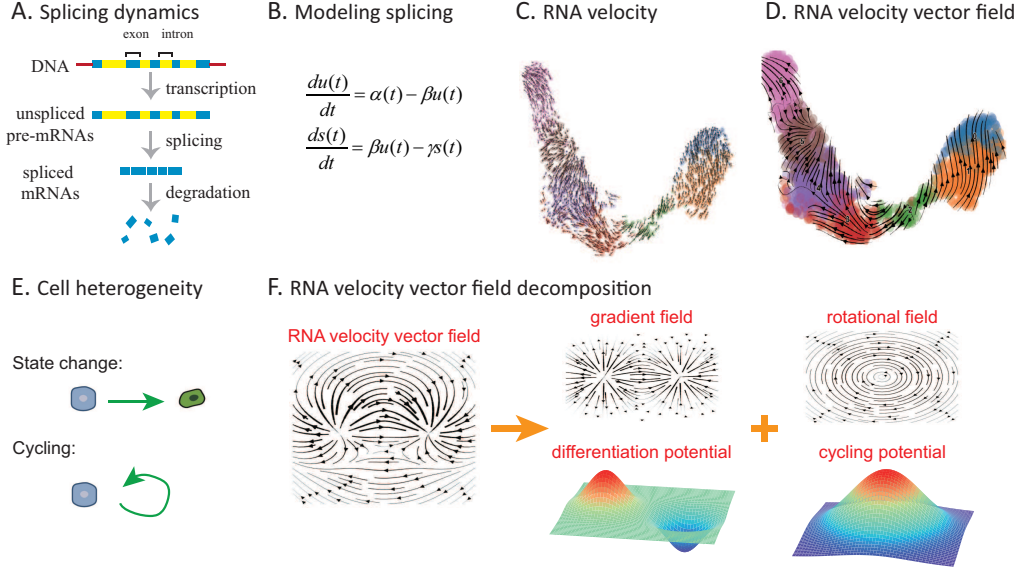


Figure 1: Schematic diagram of RNA-velocity and RNA-velocity vector field decomposition.

et al. proposed original nHHD in 2- or 3-dimensional space by separating the flows into internal and external components, which provides a unique and reliable decomposition while avoiding boundary condition constraints [Bhatia et al., 2014].

The nHHD of vector field in the n -dimensional bounded domain is described as: for any bounded domain $\Omega \subset \mathbb{R}^n$ and any twice continuously differentiable vector field $f : \Omega \rightarrow \mathbb{R}^n$ that decays faster than $\|x\|^{-c}$ for $\|x\| \rightarrow \infty$, due to internal and external influences, it is decomposed into three vector fields:

$$f(x) = g(x) + r(x) + h(x). \quad (1)$$

Where, $g(x)$ is a gradient field, where its flow emits out of the source and into the sink, and it is irrotational. $r(x)$ is a rotational field, which tends to rotate locally. And $h(x)$ is a harmonic field that has the properties both of gradient and rotational fields.

$g(x)$ and $r(x)$ are considered as natural gradient field and natural rotational field, respectively, representing the fields that are within the domain Ω and influenced by the source and rotation within this domain. However, $h(x)$ is a harmonic field, representing the field that is within the domain Ω but influenced by the exterior.

For a given domain $\Omega \subset \mathbb{R}^n$ and vector field f defined on it, the calculation of nHHD can be divided into the following three phases, as shown in Figure 2A:

1. **From vector field to densities.** Calculate the scalar source density $\gamma(x)$ and rotation density matrix $\rho(x)$ in the domain Ω :

$$\gamma(x) = \text{div} f(x) \quad (2a)$$

$$\rho(x) = \overline{\text{ROT}} f(x) = [\rho_{ij}] \quad (2b)$$

2. **From densities to potentials.** The convolution of the densities with the fundamental solution of the Laplace equation in domain Ω provides the natural source potential $G(x)$ and

the natural rotation potential matrix $R(x)$:

$$G(x) = \overline{\int_{\Omega} \gamma(x)} = \int_{\Omega} \Gamma(x-y)\gamma(y)d\omega(y) \quad (3a)$$

$$R(x) = \left[\overline{\int_{\Omega} \rho_{ij}(x)} \right] = \left[\int_{\Omega} \Gamma(x-y)\rho_{ij}(y)d\omega(y) \right] \quad (3b)$$

- 3. From potentials to vector fields.** By calculating the gradient and rotation of the corresponding potentials, the gradient field $g(x)$ and rotation field $r(x)$ can be obtained, respectively, and the remaining fields of $f(x)$ are harmonic fields $h(x)$:

$$g(x) = \text{grad}G(x) \quad (4a)$$

$$r(x) = \text{ROT}R(x) \quad (4b)$$

$$h(x) = f(x) - g(x) - r(x) \quad (4c)$$

Here, the related symbols and their meanings are shown in Supplementary Table 1. In addition, according to the above calculation phases and formulas, the densities are uniquely determined by domain Ω and vector field f , so that the potentials and their subsequent fields are also uniquely determined. Therefore, nHHD is unique.

2.2 Constructing cell differentiation potential and cycle potential by *Velde*

Previous studies on potential landscape only attempted to construct one landscape, which can be considered as potential landscape of cell differentiation. By contrast, here we will construct two potential landscapes, a cell differentiation potential landscape and a cycle potential landscape. This is mainly based on the fact that if we do not consider random factors such as external environmental disturbance and noise in expression dynamics, the heterogeneity of cells in tissues mainly comes from cell differentiation and cell cycle. Therefore, it is very appropriate to establish potential landscapes that correspond to these two processes separately.

Velde construct differentiation potential landscape and cycle potential landscape by decomposing the RNA-velocity vector field. Its input is RNA-velocity from scRNA-seq data, which can be obtained through third party libraries, such as *velocity* [La Manno et al., 2018] and *scVelo* [Bergen et al., 2020]. The results are differentiation potential landscape and cycle potential landscape. As shown in Figure 2B, the calculation process consists of three steps:

Step 1: Calculate the RNA-velocity vector field in the low-dimensional embedding space. In theory, the low-dimensional embedding space can be any embedding, but embeddings that can maintain the neighborhood relationship in the high-dimensional gene space are recommended, such as Uniform Manifold Approximation and Projection (UMAP) and t-distributed Stochastic Neighbor Embedding (t-SNE). For subsequent calculation, we use the velocity on the grid to discretize the RNA-velocity vector field, which can be obtained using the Gaussian kernel method, or firstly estimating the analytical expression of the vector field by sparse VFC and then calculating the vector field on the grid.

Step 2: Obtain the curl-free part and curl part of the RNA-velocity vector field. By the nHHD method proposed in the previous subsection, the velocity vector field is uniquely decomposed into three vector fields: gradient field $g(x)$, harmonic field $h(x)$, and rotation field $r(x)$. Since the first two fields can be explained as the cell transformation towards a direction away from its own current state, we merged these two fields to form a curl-free part to describe the cell differentiation. And the remaining rotation field serves as the curl part, which describe the cell cycle.

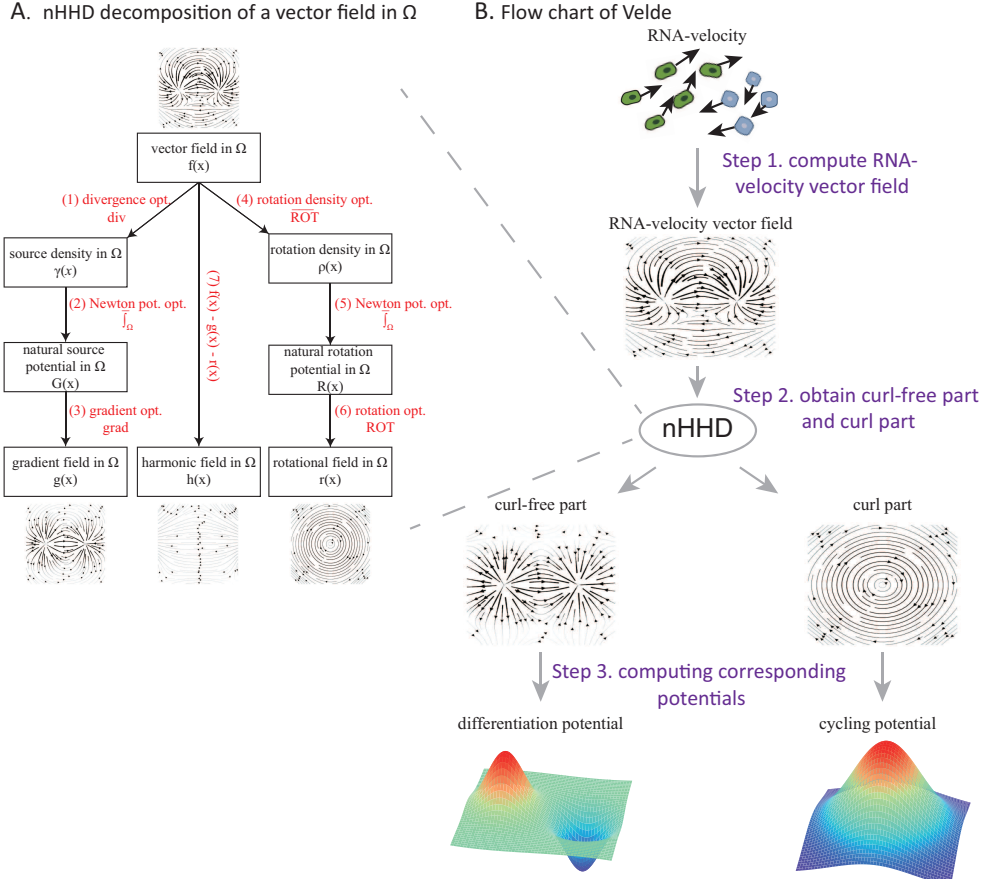


Figure 2: Natural Helmholtz-Hodge decomposition and flow chart of *Velde*.

Step 3: Calculate the differentiation potential and cycle potential. Due to the fact that the curl-free part is a superposition of a gradient field and a harmonic field, and it is still a gradient field. Therefore, theoretically, it has a corresponding source potential function, which we consider as the cell differentiation potential and it can be obtained by integrating the curl-free part. The rotational potential corresponding to the curl part serves as the cycle potential, which can be directly assigned to the natural rotational potential in the previous nHHD decomposition.

Note that the differentiation potential landscape here is the same as the usual potential landscape, describing the differentiation of cells from high potential areas to low potential areas, along the negative gradient of the landscape, $-\text{grad}G(x)$, and the greater the potential difference, the easier it is for cells to differentiate. The cell cycle potential, nevertheless, is different in that it describes the cell cycle along the direction of rotation operator, $\text{ROT}R(x)$, that is, along the clockwise contour of the cycle potential. And the steeper the cycle potential with cone-shape, the stronger the cell cycle.

3 Results

To verify the effectiveness, *Velde* was applied to both synthetic and real datasets.

3.1 Identifying hidden components of a synthetic vector field

In this subsection, we considered two synthetic datasets. The first is constructed by combining a hidden gradient vector field and a hidden rotation vector field, as shown in Figure 3. Applying *Velde* to this dataset yields an curl-free vector field and a curl vector field. The curl-free part is almost identical to the hidden gradient vector field except for some slight differences in the boundary area, and the obtained rotation part is also very similar to the hidden rotation vector field as well. This indicates that *Velde* can indeed effectively extract the hidden gradient and rotational components of the vector field.

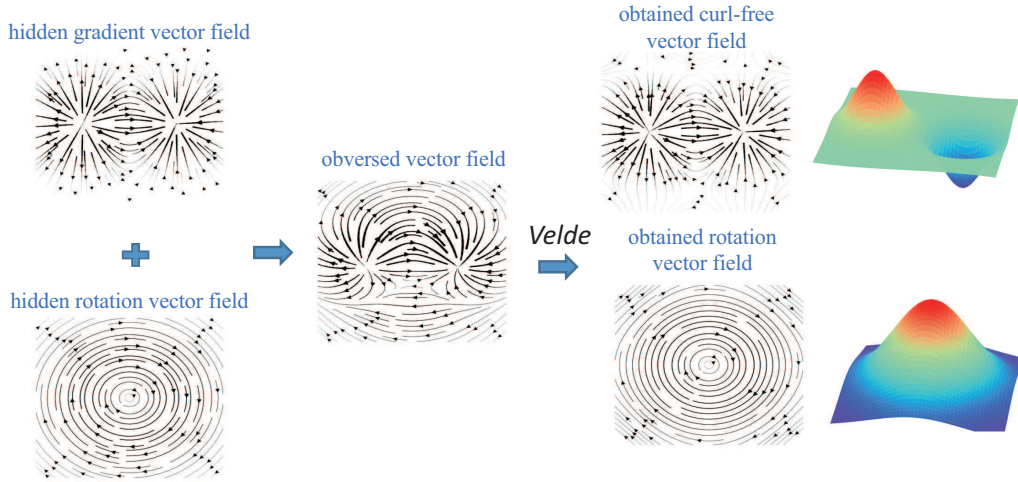


Figure 3: A synthetic vector field.

The second is a synthetic scRNA-seq dataset, with the differentiation direction of cells shown in the RNA velocity in Figure 4. By applying *Velde*, two potential landscapes were obtained, with the source potential on the left and the rotational potential on the right corresponding to the cell differentiation potential and cycle potential, respectively. From the differentiation potential landscape, it can be seen that the cells on the right generally have higher potential than the cells on the left, which is consistent with their differentiation direction. In addition, no cell regions resembling conical peaks were found within the cell population in the cycle potential landscape, indicating no obvious cell cycle.

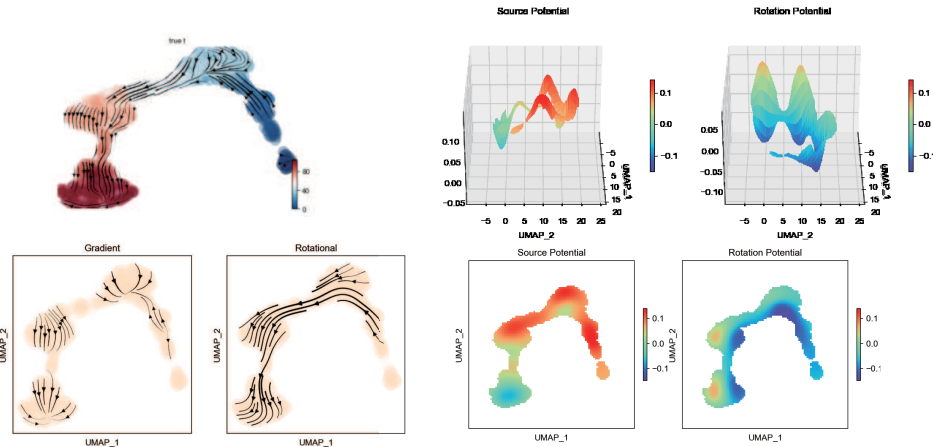


Figure 4: A synthetic scRNA-seq dataset.

3.2 Constructing cell differentiation potential and cycle potential from real datasets

We also applied *Velde* to three real scRNA-seq dataset, with the first two datasets coming from works related dentategyrus lamanno [La Manno et al., 2018] and human hematopoiesis [Qiu et al., 2022], respectively. The developmental directions and trajectories of cells are shown in the RNA velocity in the Figure 5 and 6. The differentiation potential obtained by *Velde* is consistent with the actual differentiation path of cells, and the obtained cell cycle potential also indicates that both have no obvious cell cycle.

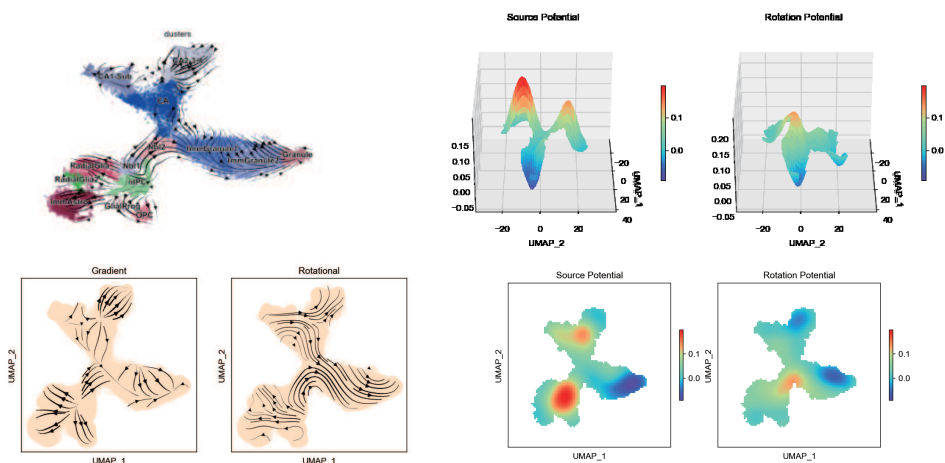


Figure 5: Dentategyrus scRNA-seq dataset [La Manno et al., 2018].

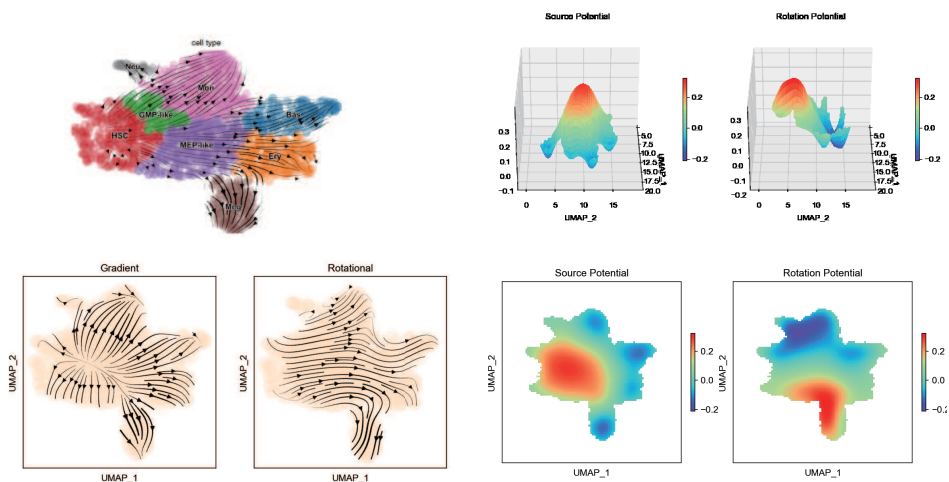


Figure 6: Human hematopoiesis scRNA-seq dataset [Qiu et al., 2022].

The third real dataset is about pancreatic development [Bastidas-Ponce et al., 2019]. Unlike the first two real datasets, this dataset not only has cell differentiation but also has strong cell cycle, as shown in Figure 7. *Velde* calculated the correct relative differentiation potential, correctly identified the cell cycle at the location of the left cells, and obtained a conical peak-shaped cell cycle potential landscape at the corresponding site.

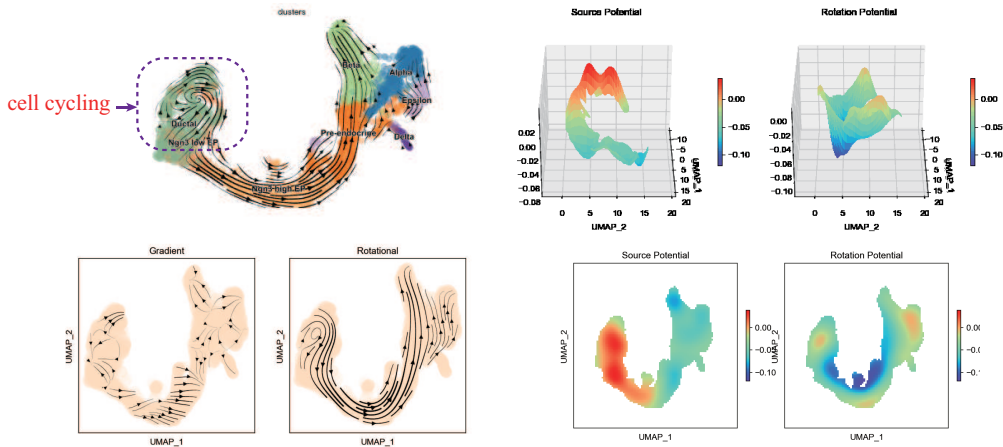


Figure 7: Pancreas scRNA-seq dataset [Bastidas-Ponce et al., 2019].

4 Conclusions and discussions

Constructing a reasonable potential landscape helps to display and understand tissue development. However, the current landscape methods only construct a cell developmental potential landscape, without considering the cell cycle associated with the cell differentiation during the development. In this article, the natural Helmholtz-Hodge decomposition of continuous vector fields on bounded domains in n -dimensional Euclidean space was proposed and a method based on this to simultaneously construct cell differentiation potential landscape and cycle potential landscape, called *Velde*, was developed as well. The effectiveness of *Velde* in calculating cell differentiation potential, identifying cell cycle, and constructing cell differentiation potential landscape and cell cycle potential landscape was verified through its application to synthetic and real datasets.

Although *Velde* can construct both cell differentiation potential and cycle potential simultaneously, its accuracy is still influenced by multiple factors. The first one is RNA velocity. Due to various noises and technical limitations during the sequencing process, there are inevitably deviations or errors in the estimating of cell RNA velocity, which directly affects the accuracy of *Velde*. The other is embedding. The reasonable layout of data points in the embedding space and whether the embedding captures the topology of cell differentiation in high-dimensional space can also affect the calculation and aesthetics of potential landscape. In addition, constructing the potential landscape is not the ultimate goal of analyzing scRNA-seq data. Based on potential landscapes, extracting the pathways involved, as well as the regulatory mechanisms between each pathway and gene is our research direction in the future.

Acknowledgements

This work was supported by the NSFC grants under Grant Nos. 12201150. We would like to thank Tiejun Li for his helpful advice and discussions.

Conflict of interest

All authors declare no conflicts of interest in this paper.

References

- [Bastidas-Ponce et al., 2019] Bastidas-Ponce, A., Tritschler, S., Dony, L., Scheibner, K., Tarquis-Medina, M., Salinno, C., Schirge, S., Burtscher, I., Böttcher, A., Theis, F. J., et al. (2019). Comprehensive single cell mrna profiling reveals a detailed roadmap for pancreatic endocrinogenesis. *Development*, 146(12):dev173849.
- [Bergen et al., 2020] Bergen, V., Lange, M., Peidli, S., Wolf, F. A., and Theis, F. J. (2020). Generalizing rna velocity to transient cell states through dynamical modeling. *Nature biotechnology*, 38(12):1408–1414.
- [Bhatia et al., 2014] Bhatia, H., Pascucci, V., and Bremer, P.-T. (2014). The natural helmholtz-hodge decomposition for open-boundary flow analysis. *IEEE transactions on visualization and computer graphics*, 20(11):1566–1578.
- [Eberwine et al., 2014] Eberwine, J., Sul, J.-Y., Bartfai, T., and Kim, J. (2014). The promise of single-cell sequencing. *Nature methods*, 11(1):25–27.
- [Glötzl and Richters, 2020] Glötzl, E. and Richters, O. (2020). Helmholtz decomposition and rotation potentials in n-dimensional cartesian coordinates. *arXiv preprint arXiv:2012.13157*.
- [Grün et al., 2016] Grün, D., Muraro, M. J., Boisset, J.-C., Wiebrands, K., Lyubimova, A., Dharmadhikari, G., van den Born, M., Van Es, J., Jansen, E., Clevers, H., et al. (2016). De novo prediction of stem cell identity using single-cell transcriptome data. *Cell stem cell*, 19(2):266–277.
- [Guo et al., 2017a] Guo, J., Lin, F., Zhang, X., Tanavde, V., and Zheng, J. (2017a). Netland: quantitative modeling and visualization of waddington’s epigenetic landscape using probabilistic potential. *Bioinformatics*, 33(10):1583–1585.
- [Guo et al., 2017b] Guo, M., Bao, E. L., Wagner, M., Whitsett, J. A., and Xu, Y. (2017b). Slice: determining cell differentiation and lineage based on single cell entropy. *Nucleic acids research*, 45(7):e54–e54.
- [H. et al., 2020] H., G. S., Bryan, I. J., A., B. D., B., K. D., and J., L. K. (2020). Applying high-dimensional single-cell technologies to the analysis of cancer immunotherapy. *Nature Reviews Clinical Oncology*, 18(4):244–256.
- [Haghverdi et al., 2016] Haghverdi, L., Büttner, M., Wolf, F. A., Buettner, F., and Theis, F. J. (2016). Diffusion pseudotime robustly reconstructs lineage branching. *Nature methods*, 13(10):845–848.
- [Jin et al., 2018] Jin, S., MacLean, A. L., Peng, T., and Nie, Q. (2018). scepath: energy landscape-based inference of transition probabilities and cellular trajectories from single-cell transcriptomic data. *Bioinformatics*, 34(12):2077–2086.
- [La Manno et al., 2018] La Manno, G., Soldatov, R., Zeisel, A., Braun, E., Hochgerner, H., Petukhov, V., Lidschreiber, K., Kastrioti, M. E., Lönnerberg, P., Furlan, A., et al. (2018). Rna velocity of single cells. *Nature*, 560(7719):494–498.
- [Lim et al., 2023] Lim, J., Chin, V., Fairfax, K., Moutinho, C., Suan, D., Ji, H., and Powell, J. E. (2023). Transitioning single-cell genomics into the clinic. *Nat Rev Genet*, 24(8):573–584.
- [Luecken and Theis, 2019] Luecken, M. D. and Theis, F. J. (2019). Current best practices in single-cell rna-seq analysis: a tutorial. *Molecular systems biology*, 15(6):e8746.
- [Ma et al., 2013] Ma, J., Zhao, J., Tian, J., Bai, X., and Tu, Z. (2013). Regularized vector field learning with sparse approximation for mismatch removal. *Pattern Recognition*, 46(12):3519–3532.

- [Qiu et al., 2017] Qiu, X., Mao, Q., Tang, Y., Wang, L., Chawla, R., Pliner, H. A., and Trapnell, C. (2017). Reversed graph embedding resolves complex single-cell trajectories. *Nature methods*, 14(10):979–982.
- [Qiu et al., 2022] Qiu, X., Zhang, Y., Martin-Rufino, J. D., Weng, C., Hosseinzadeh, S., Yang, D., Pogson, A. N., Hein, M. Y., Min, K. H. J., Wang, L., et al. (2022). Mapping transcriptomic vector fields of single cells. *Cell*, 185(4):690–711.
- [Rood et al., 2022] Rood, J. E., Maartens, A., Hupalowska, A., Teichmann, S. A., and Regev, A. (2022). Impact of the human cell atlas on medicine. *Nature Medicine*, 28(12):2486–2496.
- [Setty et al., 2016] Setty, M., Tadmor, M. D., Reich-Zeliger, S., Angel, O., Salame, T. M., Kathail, P., Choi, K., Bendall, S., Friedman, N., and Pe’er, D. (2016). Wishbone identifies bifurcating developmental trajectories from single-cell data. *Nature biotechnology*, 34(6):637–645.
- [Shi et al., 2019] Shi, J., Li, T., Chen, L., and Aihara, K. (2019). Quantifying pluripotency landscape of cell differentiation from scRNA-seq data by continuous birth-death process. *PLoS computational biology*, 15(11):e1007488.
- [Shi et al., 2020] Shi, J., Teschendorff, A. E., Chen, W., Chen, L., and Li, T. (2020). Quantifying Waddington’s epigenetic landscape: a comparison of single-cell potency measures. *Briefings in bioinformatics*, 21(1):248–261.
- [Tang et al., 2009] Tang, F., Barbacioru, C., Wang, Y., Nordman, E., Lee, C., Xu, N., Wang, X., Bodeau, J., Tuch, B. B., Siddiqui, A., et al. (2009). mRNA-seq whole-transcriptome analysis of a single cell. *Nature methods*, 6(5):377–382.
- [Teschendorff and Enver, 2017] Teschendorff, A. E. and Enver, T. (2017). Single-cell entropy for accurate estimation of differentiation potency from a cell’s transcriptome. *Nature communications*, 8(1):15599.
- [Teschendorff and Feinberg, 2021] Teschendorff, A. E. and Feinberg, A. P. (2021). Statistical mechanics meets single-cell biology. *Nature Reviews Genetics*, 22(7):459–476.
- [Trapnell et al., 2014] Trapnell, C., Cacchiarelli, D., Grimsby, J., Pokharel, P., Li, S., Morse, M., Lennon, N. J., Livak, K. J., Mikkelsen, T. S., and Rinn, J. L. (2014). The dynamics and regulators of cell fate decisions are revealed by pseudotemporal ordering of single cells. *Nature biotechnology*, 32(4):381–386.
- [Tusi et al., 2018] Tusi, B. K., Wolock, S. L., Weinreb, C., Hwang, Y., Hidalgo, D., Zilionis, R., Waisman, A., Huh, J. R., Klein, A. M., and Socolovsky, M. (2018). Population snapshots predict early haematopoietic and erythroid hierarchies. *Nature*, 555(7694):54–60.
- [Waddington, 1957] Waddington, C. H. (1957). *The Strategy of the Genes, a Discussion of Some Aspects of Theoretical Biology*. G. Allen and Unwin.
- [Wang et al., 2010] Wang, J., Li, C., and Wang, E. (2010). Potential and flux landscapes quantify the stability and robustness of budding yeast cell cycle network. *Proceedings of the National Academy of Sciences*, 107(18):8195–8200.

A Supplementary information

A.1 Supplementary Table 1: symbols and meanings

Table 1: Some variables and operators along with corresponding explanations

Variable or Operator	Explanation
vector field $f \in C^2(\mathbb{R}^n, \mathbb{R}^n)$	$f(x) = (f_k(x); 1 \leq k \leq n)$
divergence operator $\text{div} : C^1(\mathbb{R}^n, \mathbb{R}^n) \rightarrow C^0(\mathbb{R}^n, \mathbb{R})$	$\text{div} f(x) = \sum_{i=1}^n \frac{\partial f_i(x)}{\partial x_i}$
scalar source density $\gamma \in C^1(\mathbb{R}^n, \mathbb{R})$	$\gamma(x) = \text{div}(x)$
Newton potential operator $\bar{\int} : C^0(\mathbb{R}^n, \mathbb{R}) \rightarrow C^1(\mathbb{R}^n, \mathbb{R})$	$\bar{\int} \gamma(x) := \Gamma(x) * \gamma(x) = \int_{\mathbb{R}^n} \Gamma(x-y) \gamma(y) d\omega(y)$
scalar source potential $G \in C^1(\mathbb{R}^n, \mathbb{R})$	$G(x) = \bar{\int} \gamma(x)$
gradient operator $\text{grad} : C^1(\mathbb{R}^n, \mathbb{R}) \rightarrow C^0(\mathbb{R}^n, \mathbb{R}^n)$	$\text{grad} G(x) = \left(\frac{\partial G(x)}{\partial x_k}; 1 \leq k \leq n \right)$
basic rotation density operator $\overline{\text{ROT}}_{ij} : C^1(\mathbb{R}^n, \mathbb{R}^n) \rightarrow C^0(\mathbb{R}^n, \mathbb{R})$	$\overline{\text{ROT}}_{ij} f(x) := \frac{\partial f_i(x)}{\partial x_j} - \frac{\partial f_j(x)}{\partial x_i}$
rotation density operator $\overline{\text{ROT}} : C^1(\mathbb{R}^n, \mathbb{R}^n) \rightarrow C^0(\mathbb{R}^n, \mathbb{R}^{n^2})$	$\overline{\text{ROT}} f(x) := [\overline{\text{ROT}}_{ij} f(x)] = \left[\frac{\partial f_i(x)}{\partial x_j} - \frac{\partial f_j(x)}{\partial x_i}; 1 \leq i, j \leq n \right]$
basic rotation density $\rho_{i,j} \in C^1(\mathbb{R}^n, \mathbb{R})$	$\rho_{ij}(x) = -\rho_{ji}(x) = \overline{\text{ROT}}_{ij} f(x); 1 \leq i, j \leq n$
rotation density $\rho \in C^1(\mathbb{R}^n, \mathbb{R}^{n^2})$	$\rho(x) = [\rho_{ij}(x); 1 \leq i, j \leq n] = \overline{\text{ROT}} f(x)$
basic rotation potentials $R_{ij} \in C^3(\mathbb{R}^n, \mathbb{R})$	$R_{ij}(x) = \bar{\int} \rho_{ij}(x); 1 \leq i, j \leq n$
rotation potential $R \in C^3(\mathbb{R}^n, \mathbb{R}^{n^2})$	$R(x) = [R_{ij}(x); 1 \leq i, j \leq n]$
basic rotation operator $\text{ROT}_{ij} : C^1(\mathbb{R}^n, \mathbb{R}) \rightarrow C^0(\mathbb{R}^n, \mathbb{R}^n)$	$\text{ROT}_{ij} R_{ij}(x) = \left(\delta_{ik} \frac{\partial R_{ij}(x)}{\partial x_j} - \delta_{jk} \frac{\partial R_{ij}(x)}{\partial x_i}; 1 \leq k \leq n \right)$
rotation operator $\text{ROT} : C^1(\mathbb{R}^n, \mathbb{R}^{n^2}) \rightarrow C^0(\mathbb{R}^n, \mathbb{R}^n)$	$\text{ROT} R := \sum_{1 \leq i, j \leq n} \frac{1}{2} \text{ROT}_{ij} R_{ij}(x) = \left(\sum_m \frac{\partial R_{km}(x)}{\partial x_m}; 1 \leq k \leq n \right)$

A.2 Supplementary Figure 1: schematic diagram of HHD

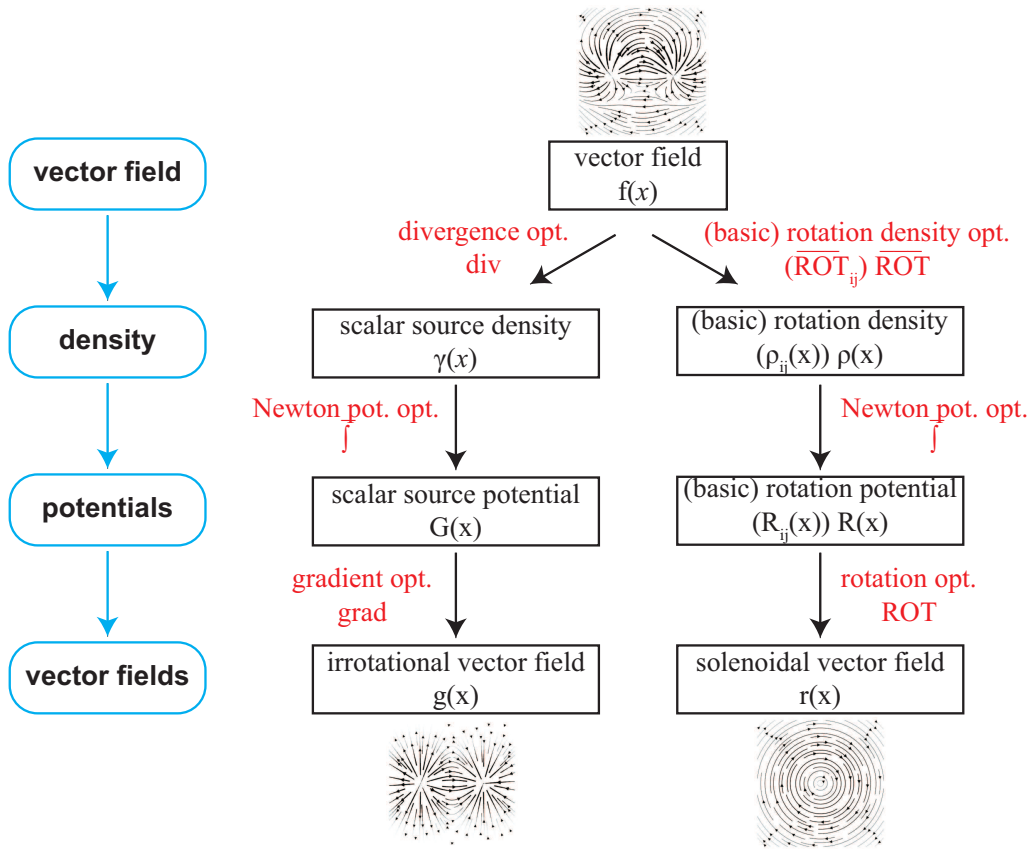


Figure 8: Schematic diagram of Helmholtz-Hodge Decomposition of vector field in \mathbb{R}^n .